molbank

MDPI

Communication

N-(*p*-Toluenesulfonyl)-1-(4′-acetylphenoxy)acrylimidate: Synthesis, Crystal Structure and Theoretical Studies

Flor María Escandón-Mancilla [1,2], Alberto Cedillo-Cruz [1,2], Raúl Eduardo Gordillo-Cruz [1,2], Diego Martínez-Otero [1,3], M. V. Basavanag Unnamatla [1,2] and Erick Cuevas-Yañez [1,2,*]

1 Centro Conjunto de Investigación en Química Sustentable UAEM-UNAM, Universidad Autónoma del Estado de México, Carretera Toluca-Atlacomulco Km 14.5, Toluca 50200, Mexico
2 Facultad de Química, Universidad Autónoma del Estado de México, Paseo Colon esq. Paseo Tollocan, Toluca 50120, Mexico
3 Instituto de Química, Universidad Nacional Autónoma de México, Circuito Exterior S. N., Ciudad Universitaria, Coyoacán, Ciudad de México 04510, Mexico
* Correspondence: ecuevasy@uaemex.mx; Tel.: +52-722-276-6610 (ext. 7734); Fax: +52-722-217-5109

Abstract: The formation of N-sulfonyl-1-aryloxy acrylimidate is described, for the first time, from a consecutive process, which involves a CuAAC reaction, a ketenimine formation and subsequent rearrangement between an aryl propargyl ether and a sulfonyl azide. The structure of this newly synthesized compound was analyzed by NMR spectra and unambiguously established by X-ray analysis. In addition, theoretical calculations, which included a Hirshfeld surface, FMO, QTAIM and NCI indices analysis, corroborated the formation of π-π stacking interactions among aromatic rings, as well as C-H···O interactions between vinyl hydrogens with ketone carbonyl oxygen.

Keywords: acrylimidate; sulfonyl azide; ketenimine; CuAAC reaction; crystal structure

Citation: Escandón-Mancilla, F.M.; Cedillo-Cruz, A.; Gordillo-Cruz, R.E.; Martínez-Otero, D.; Unnamatla, M.V.B.; Cuevas-Yañez, E. *N*-(*p*-Toluenesulfonyl)-1-(4′-acetylphenoxy)acrylimidate: Synthesis, Crystal Structure and Theoretical Studies. *Molbank* **2022**, *2022*, M1509. https://doi.org/10.3390/M1509

Academic Editor: Hideto Miyabe

Received: 2 August 2022
Accepted: 24 September 2022
Published: 28 November 2022

1. Introduction

The number of applications of copper-catalyzed azide-alkyne cycloaddition (CuAAC) is not only limited to the preparation of 1,2,3-tiazoles, but has also been extended to the generation of interesting intermediates, such as ketenimines. In this regard, seminal works of Chang and coworkers [1] demonstrated the potential of this reaction in the preparation of compounds of chemical interest [2].

In connection with other synthetic studies, some time ago we investigated new methods and catalysts for selective preparation of 1-sulfonyl-1,2,3-triazoles from sulfonyl azides and alkynes [3–5]. Derived from these studies, and as an effort to expand the uses of this reaction to other systems, we found the formation of an unexpected product from an aryl propargyl ether and a sulfonyl azide under conventional CuAAC reaction conditions. Herein is described our most recent results in this area.

2. Results and Discussion

In this report, we disclose that straightforward treatment of p-toluenesulfonyl azide **2** and 1-(4-prop-2-ynyloxyphenyl)ethanone **1** in the presence of catalytic amounts of copper(I) salicylate [5] afforded N-(p-toluenesulfonyl)-1-(4′-Acetylphenoxy)acrylimidate **3** in 29% yield, as depicted in Scheme 1.

An important spectroscopic feature, which gave rise to the product identification, was a signal pattern observed in the ^{1}H NMR spectrum associated with a vinyl system, see Figure 1 (Supplementary Materials), with two doublet signals at δ 6.18 ppm (J_{ac} = 10.89 Hz) and 6.67 ppm (J_{ab} = 16.98 Hz), assigned to geminal hydrogens, as well as a doublet of doublets signal at δ 7.39 ppm (J_{ab} = 16.95 Hz and J_{ac} = 10.86 Hz), corresponding to Hydrogen on C-2 from acrylimidate moiety. On the other hand, vinyl carbon signals were located at δ

113.2 and 127.2 ppm in ^{13}C NMR, whereas an imidate C=N carbon signal was observed at δ 195.1 ppm (Figure 2).

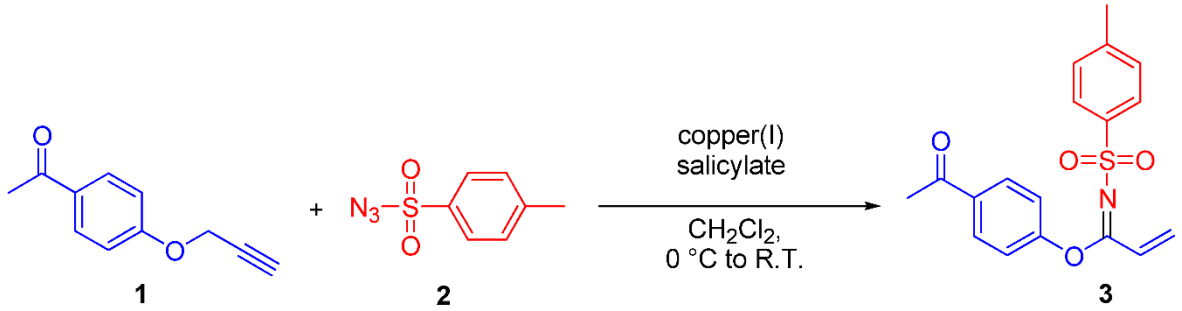

Scheme 1. Formation of N-(p-toluenesulfonyl)-1-(4′-Acetylphenoxy)acrylimidate **3**.

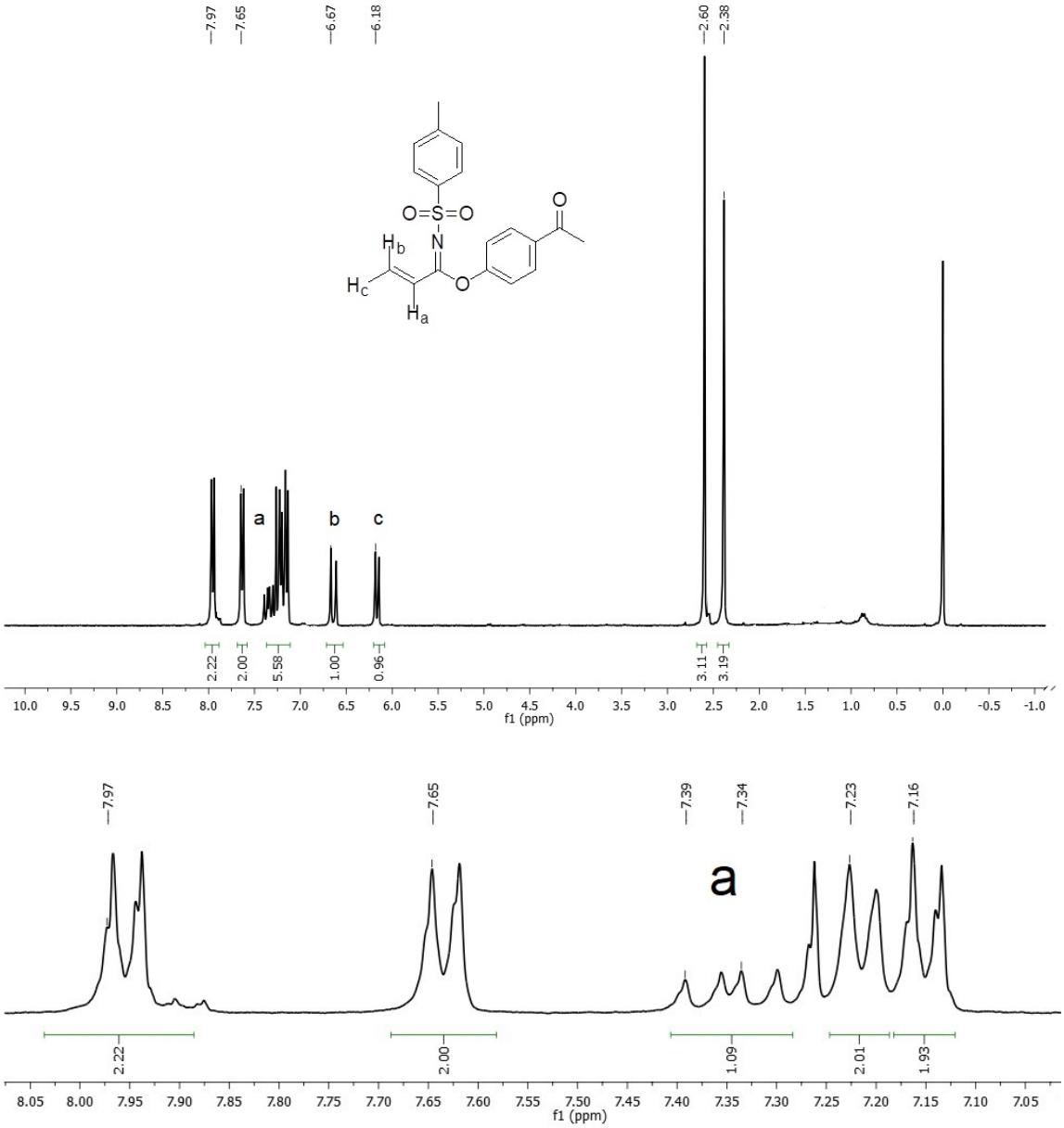

Figure 1. ^{1}H NMR spectrum of imidate **3**.

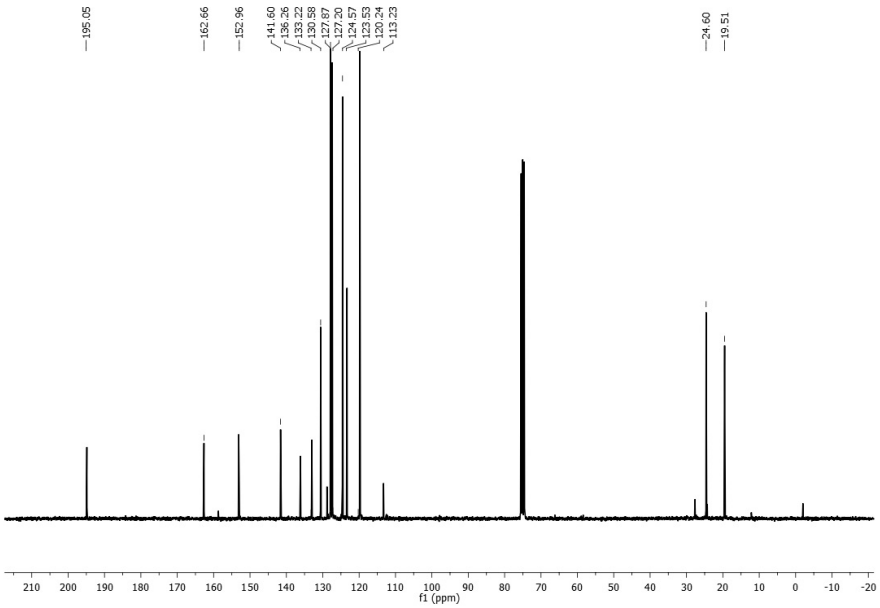

Figure 2. ^{13}C-NMR spectrum of imidate **3**.

The structure of imidate **3** was unambiguously elucidated by X-ray crystallography. due to compound **3** resulting in a crystalline solid. Crystallographic data and structural refinement parameters of **3** are summarized in Table 1, and the crystal structure of compound **3** is projected in Figure 3. A notable U-shaped conformation was perceived, similar to those observed in certain aromatic urea dicarboxylic acids [6] and helicenes [7]. For compound **3**, the aromatic rings underwent an approaching which could be evidenced by distances up to 2.944 Å between hydrogens in the toluenesulfonyl ring with hydrogens in the acetyl phenoxy system. Moreover, these rings maintained an almost perpendicular position, displaying a dihedral angle of 85.69°.

Table 1. Crystallographic data for structural analysis of compound **3**.

Crystal Data	**3**
Empirical formula	$C_{18}H_{17}NO_4S$
Formula weight	343.38
Temperature (K)	100(2)
Radiation type	Mo Kα
Crystal system	Triclinic
Space group	$P-1$
Unit cell dimensions (Å, °)	
a	9.1339(4)
b	9.4474(4)
c	10.7404(4)
α	66.3790(10)
β	85.4950(10)
γ	77.8620(10)
Volume (Å^3)	830.15(6)
Z	2
Density (calculated, Mg/m^3)	1.374
Absorption coefficient μ (mm^{-1})	0.217
F(000)	360
Crystal size (mm^3)	0.160 × 0.185 × 0.318
Θ range (deg)	2.070 to 27.504
Index ranges	$-11 \leq h \leq 11$, $-12 \leq k \leq 12$, $-13 \leq l \leq 13$
Reflections collected	18,221
Independent reflections	3808 [R(int) = 0.0130]
Data/restraints/parameters	3808/0/219
Goodness-of-fit on F2	1.039
Final R indices [I > 2sigma(I)]	R1 = 0.0298, wR2 = 0.0805
R indices (all data)	R1 = 0.0306, wR2 = 0.0812
Largest diff. peak and hole (e Å^{-3})	0.435, −0.390

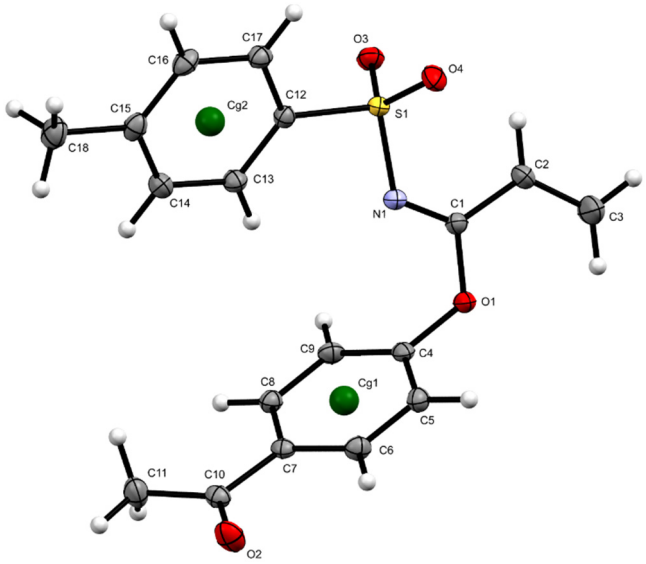

Figure 3. Geometric structures of **3** obtained by X-ray diffraction, displacement ellipsoids are drawn at the 50% probability level.

The above-described conformation was probably due to the presence of diverse interactions, highlighting π-π stacking interactions, a first Cg1···Cg1 interaction with a distance of 3.8729(7) Å (symmetry code −x + 1, −y + 1, −z) and a second Cg2···Cg2 interaction with a distance of 4.8878(7) Å (symmetry code −x + 2, −y + 1, −z + 1), as seen in Table 2 and Figure 4, and C-H···O interactions between vinyl hydrogens with ketone carbonyl oxygen (distances C3-H···O = 2.561 Å and C2-H···O 2.592 Å) which, in turn, also interacted with an aromatic hydrogen from tosyl moiety, C14-H···O = 2.703 Å, as well as with aromatic hydrogens from the outer acetyl phenoxy ring C8-H···O = 2.770 Å and C9-H···O = 2.922 Å.

Table 2. Hydrogen-bond geometry (Å, °).

D—H···*A*	*D*—H	H···*A*	*D*···*A*	*D*—H···*A*
C2—H2···O2 [i]	0.95	2.59	3.2198(14)	123.9
C3—H3B···O2 [i]	0.95	2.56	3.1986(16)	124.7
C2—H2···O3	0.95	2.71	3.2620(14)	117.3
C13—H13···N1	0.95	2.45	2.8398(14)	104.4
C11—H11A···O4 [ii]	0.98	2.63	3.5461(16)	155.5
C11—H11B···O3 [iii]	0.98	2.85	3.6760(15)	142.8
C17—H17···O3 [iv]	0.95	2.78	3.7080(14)	164.4
C9—H9···Cg2 [iii]	0.95	2.55	3.4644(12)	162.9

Symmetry codes: (i) x − 1, y + 1, z; (ii) x, y − 1, z; (iii) −x + 1, −y + 1, −z + 1; (iv) −x + 1, −y + 2, −z + 1.

A subsequent Hirshfeld surface analysis was determined on compound **3**. A projection of the Hirshfeld surfaces for imidate **3** mapped over d_{norm} (top and bottom), d_i, d_e, shape index and curvedness are plotted in Figures 5 and 6, displaying red spots which indicate high-intensity contacts and closest interactions being located on vinyl hydrogens along with hydrogens from both aromatic rings. These contact zones exhibited significant C-H···O hydrogen interactions, as seen in Figure 7. Furthermore, 2D fingerprint plots of d_e versus d_i for compound **3** (Figure 8) allowed a visualization of hydrogen bonded interactions with C and O atoms, noting an important contribution by H···H (41.1%) and O···H (29.1%) contacts, confirming previous observations.

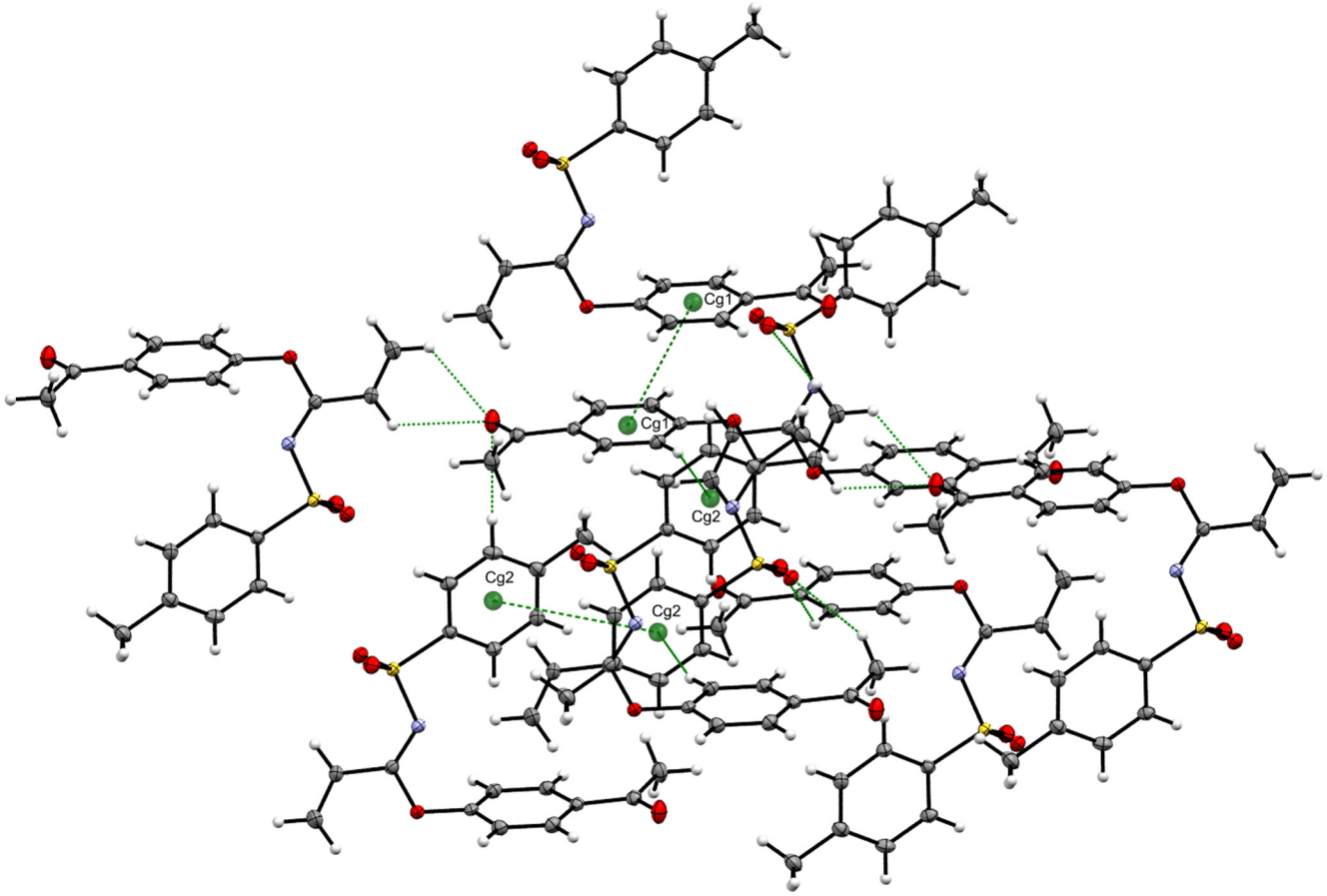

Figure 4. C-H···O, C-H···π and π-π stacking interactions found in imidate **3**.

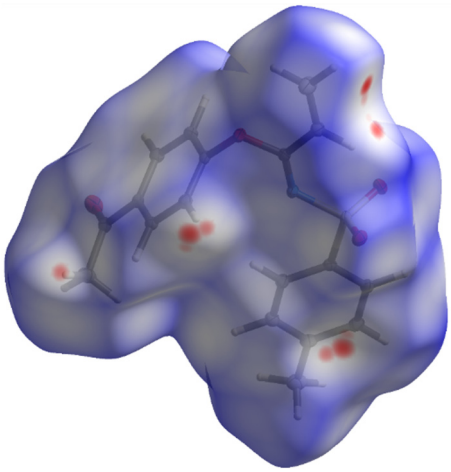

Figure 5. Hirshfeld surface for **3** with d_{norm} in the range −0.0768 to 1.2478 a.u.

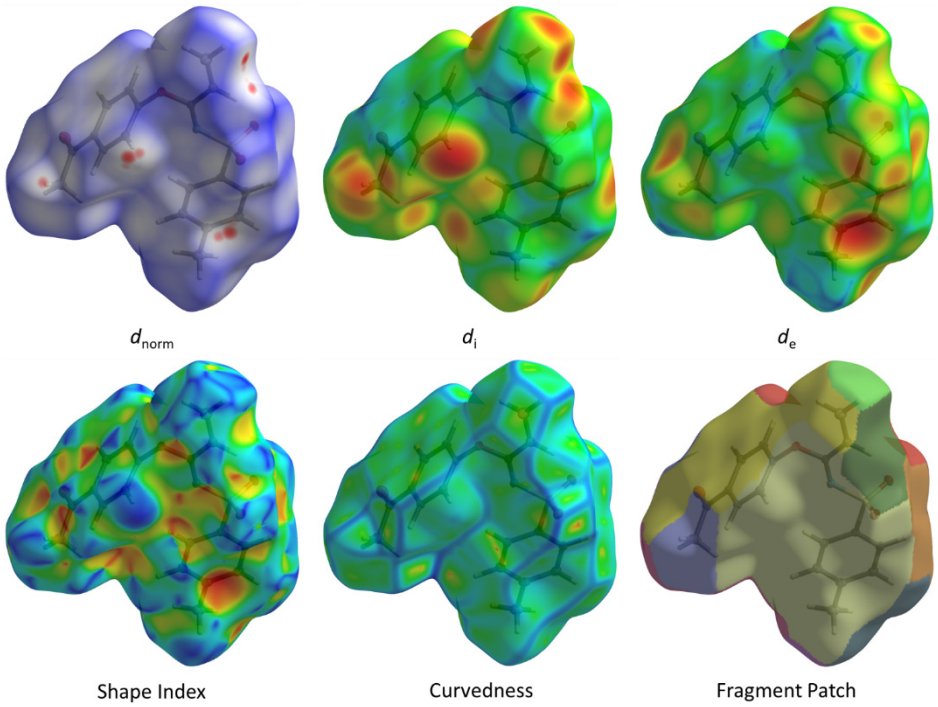

Figure 6. Hirshfeld surface for **3** with d_{norm}, d_i, d_e, shape index, curvedness and fragment patch.

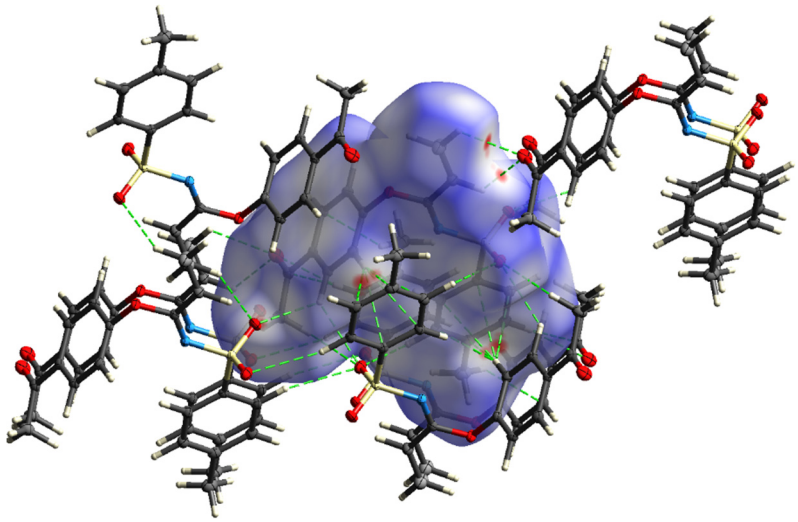

Figure 7. Hirshfeld surface of **3** mapped with d_{norm}, showing potential hydrogen bond (dashed lines).

As a complement of the aforementioned, a topology study was carried out, which included both quantum theory of atoms in molecules (QTAIM) as well as non-covalent interaction (NCI) index. A graphical overview is presented in Figure 9, covering graphical representations of QTAIM through Bond Critical Point (BCP), Critical Ring Point (RCP) and Critical Cage Point (CCP), which are indicated in orange, yellow and green colors, respectively. In the case of NCI, the blue and green iso-surfaces were placed around aromatic ring bonds, pointing out an outstanding π-π stacking contact. In consequence, these studies agreed with the crystallographic information.

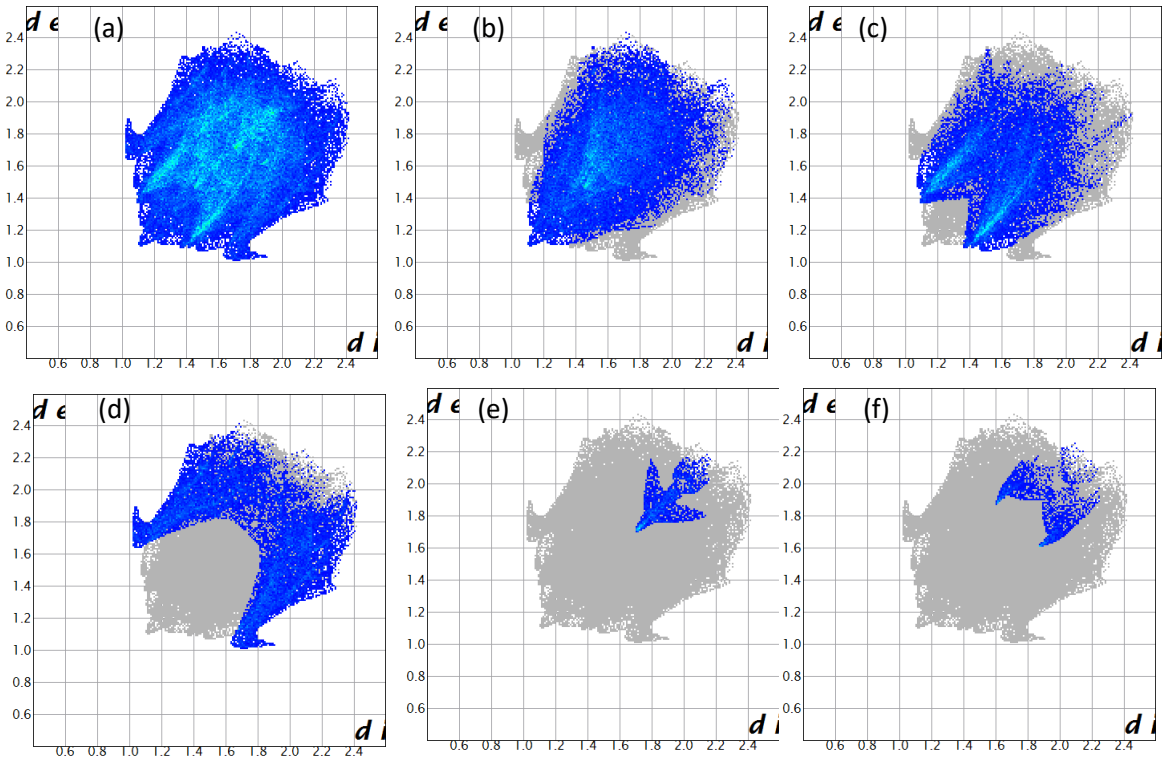

Figure 8. Two-dimensional fingerprint plots for compound **3**, showing (**a**) all interactions, and delineated into (**b**) H···H (41.1%), (**c**) H···O/O···H (29.1%), (**d**) H···C/C···H (22.3%), (**e**) C···C (2.8%) and (**f**) C···O/O···C (2.2%) interactions.

A frontier molecular orbital (FMO) analysis for molecule **3** was verified; the HOMO and LUMO energies were calculated at PBE1PBE/cc-pVDZ level for gaseous phase. From these calculations, a LUMO–HOMO energy gap value of −5.150 eV for **3** was determined. The FMO diagrams are plotted in Figure 10 and HOMO and LUMO energy values, in conjunction with some other molecular properties, are shown in Table 3.

Table 3. HOMO-LUMO energies and values of quantum chemical parameters calculated at PBE1PBE/cc-pVDZ level of theory.

Crystal Data	3
Etotal (a.u.)	−1448.480
ELUMO (eV)	−1.956
EHOMO (eV)	−7.106
Electron affinity (eV)	1.956
Ionization potential (eV)	7.106
Gap Energy (eV)	5.150
Electronegativity (eV)	4.531
Chemical hardness (eV)	2.575
Chemical softness (eV^{-1})	0.388
Chemical potential (eV)	−4.531
Electrophilicity index (eV)	3.986

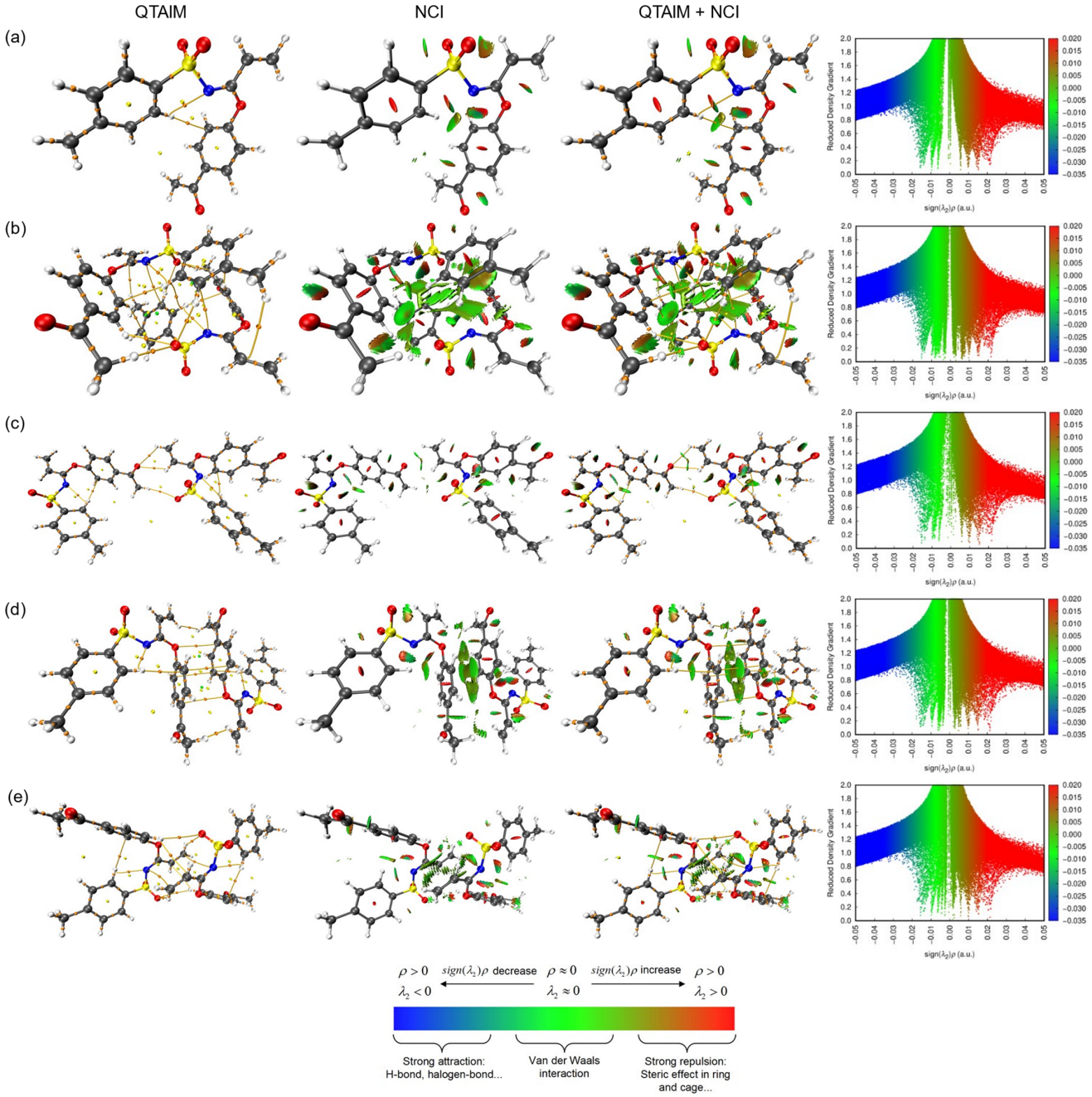

Figure 9. Weak interactions analyzed by QTAIM and NCI index (iso-surface 0.5 a.u.) for monomer (**a**) and dimers (**b**–**e**) of **3**, bond critical points (3, −1) in orange, ring critical points (3, +1) in yellow and cage critical points (3, +3) in green.

Calculation of local reactivity descriptors, such as electron affinity (A), ionization potential (I), gap energy, electronegativity (χ), chemical hardness (η), chemical softness (ζ), chemical potential (μ) and electrophilicity index (ω) results were helpful in the interpretation of Molecular Electrostatic Potential surfaces (MEP), which are mapped in Figure 11. In this regard, MEP projected upon an electron density iso-surface of imidate **3** was in the range $\pm 5.414 \cdot 10^{-2}$, displaying negative charge distributions marked in red upon oxygen atoms from both carbonyl and sulfonyl groups. This charge distribution was also observed in the respective electronegative electrostatic potential (ESP) surface indicated in the blue color in Figure 12. This was an important finding, because negative charge distributions enable the referred C-H···O interactions.

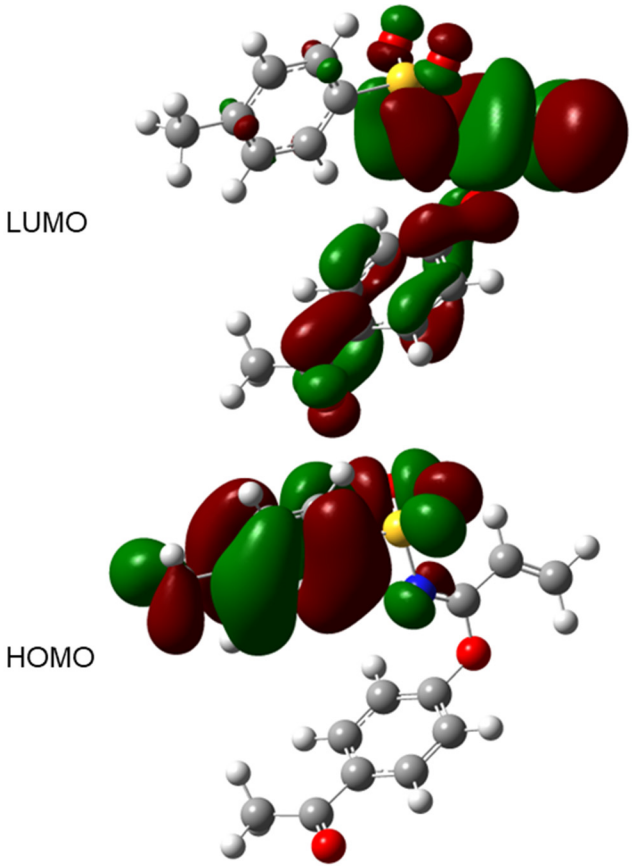

Figure 10. LUMO and HOMO plot (iso-surface 0.02 a.u.) for **3** calculated at PBE1PBE/cc-pVDZ level of theory.

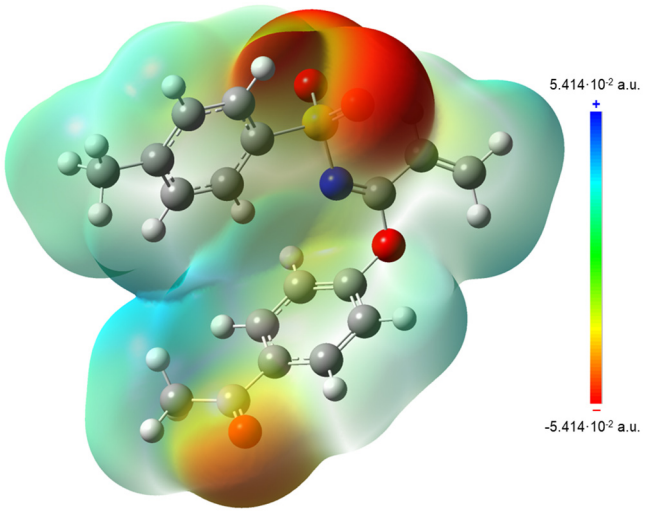

Figure 11. MEP surface (iso-surface 0.0004 a.u.) for **3** calculated at PBE1PBE/cc-pVDZ level of theory.

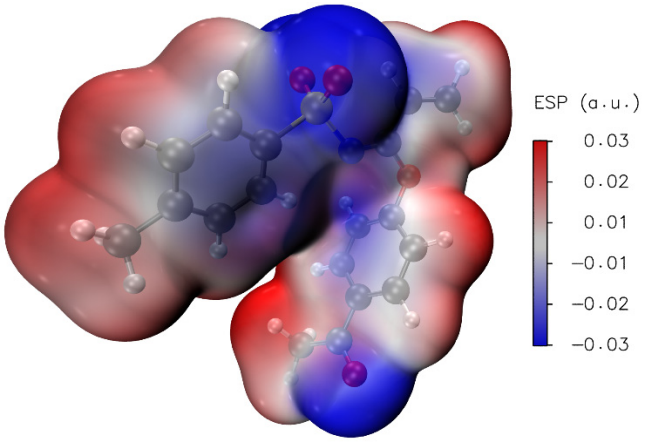

Figure 12. ESP (iso-surface 0.001 a.u.) for **3** calculated at PBE1PBE/cc-pVDZ level of theory.

The formation of imidate **3** can be rationalized in terms of a reaction mechanism described in Scheme 2. Cycloaddition between aryloxy alkyne **4** and sulfonyl azide **2** in the presence of a catalytic cuprous source produces copper triazolide **5,** which is cleaved into diazo imine **6,** that, after nitrogen extrusion, gives ketenimine **8,** which undergoes a rearrangement to afford the final imidate **3**.

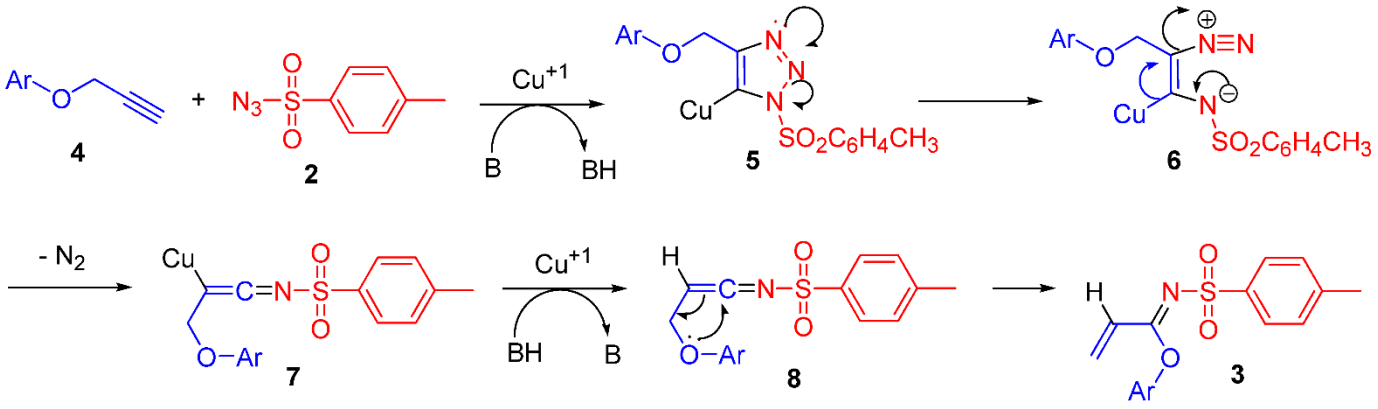

Scheme 2. Plausible formation mechanism of imidate **3**.

Few examples of similar processes have been reported in literature. Acetate group migration was detected in the synthesis of trans-α,β-unsaturated N-tosylamides from p-toluenesulfonyl azide and diverse propargyl acetates in [8,9]. On the flip side, a set of acrylamidines was prepared from the corresponding N,N-dialkyl propargylamines through a 1,3-amino group migration on ketenimine intermediates in [10]. Hence, this is the first example concerning an intramolecular aryloxy ketenimine rearrangement; wherefore, future investigations will be driven to study in more detail this process and to broaden the synthetic applications of this kind of intermediate.

3. Materials and Methods

The starting materials were purchased from Aldrich Chemical Co. and were used without further purification. Copper(I) salicylate was prepared according to literature [5]. The solvents were distilled before use. Silica plates of 0.20 mm thickness were used for thin layer chromatography. Melting points were determined with a Krüss Optronic melting point apparatus, and they were uncorrected. ^{1}H and ^{13}C NMR spectra were recorded using a Bruker Avance 300-MHz; the chemical shifts (δ) are given in ppm relative to TMS as an internal standard (0.00). For analytical purposes, the mass spectra were recorded on a Shimadzu GCMS-QP2010 Plus in the EI mode, 70 eV, and 200 °C via direct inlet probe.

Only the molecular and parent ions (m/z) are reported. IR spectra were recorded on a Bruker Tensor 27 (Supplementary Materials).

For the X-ray diffraction studies, crystals of compound **3** were obtained by slow evaporation of a dilute AcOEt solution, and the reflections were acquired with a Bruker APEX DUO diffractometer equipped with an Apex II CCD detector, Mo Kα radiation (λ = 0.71073 Å) at 100 K. Frames were collected using omega scans and integrated with SAINT and multi-scan absorption correction (SADABS) was applied [11]. The structure was solved by direct methods (SHELXS-97) [12]; missing atoms were found by difference-Fourier synthesis and refined on F2 by a full-matrix least-squares procedure using anisotropic dis-placement parameters using SHELXL [13] using the ShelXle GUI [14]. The hydrogen atoms of the C–H bonds were placed in idealized positions. The molecular graphics were prepared using Mercury [15] and POV-Ray [16]. Crystallographic data for the structure reported in this paper have been deposited with the Cambridge Crystallographic Data Centre, CCDC No. 2183265 for compound **3**. Copies of available materials can be obtained free of charge on application to the Director, CCDC, 12 Union Road, Cambridge CB2 IEZ, UK (facsimile: (44) 01223 336033); e-mail: deposit@ccdc.ac.uk.

The quantum chemical calculations were performed using Gaussian 09 program package [17]. The crystal structure geometry was used as a starting model to optimize. The vibration frequencies were calculated for the optimized structure in gas phase and no imaginary frequencies were obtained. All calculations were done at PBE1PBE/cc-pVDZ level of theory [18–20].

The Hirshfeld surface mapped with d_{norm} and fingerprint plots were performed with Crystal Explorer 21.5 program [21]. The 2-D fingerprint plots were used for visualizing, exploring and quantifying intermolecular interactions.

The Quantum Theory of Atoms in Molecules (QTAIM) [22] and non-covalent interactions (NCI) [23] analysis have been performed using Multiwfn 3.8 [24] at PBE1PBE/cc-pVDZ level of theory on the structures of **1** (monomer or dimer) in which only the positions of the hydrogen atoms were optimized. The VMD 1.9.4 [25] and GNUplot 5.4 [26] were used for the visualization of the results.

*Synthesis of N-(p-Toluenesulfonyl)-1-(4′-acetylphenoxy)acrylimidate **3***

1-(4-Prop-2-ynyloxyphenyl)ethanone **1** (0.174 g, 1.0 mmol) was added in one portion to a solution of p-toluenesulfonyl azide **2** (0.197 g, 1.0 mmol) and copper (I) salicylate (0.0099 g, 0.05 mmol) in CH_2Cl_2 (6 mL) at 0 °C. The resulting mixture was stirred at 0 °C for 3 h and at room temperature for 3 h. Charcoal (0.05 g) was added, the mixture was filtered through celite, and the solvent was removed under reduced pressure. Purification by column chromatography (SiO_2, hexane/AcOEt 8:2) afforded N-(p-toluenesulfonyl)-1-(4′-acetylphenoxy)acrylimidate **3** (0.099 g, 29%) as a colorless oil. ^{1}H NMR (300 MHz, $CDCl_3$) δ 7.97 (d, J = 8.7 Hz, 2H), 7.65 (d, J = 8.1 Hz, 2H), 7.39 (dd, J_{ab} = 16.95 Hz, J_{ac} = 10.86 Hz, 1H), 7.23 (d, J = 8.1 Hz, 2H), 7.16 (d, J = 8.7 Hz, 2H), 6.67 (d, J_{ab} = 16.98 Hz, 1H), 6.18 (d, J_{ac} = 10.89 Hz, 1H), 2.60 (s, 3H), 2.38 (s, 3H); ^{13}C NMR (75 MHz, $CDCl_3$) δ 195.0 (C), 162.7 (C), 153.3 (C), 141.6 (C), 136.3 (C), 133.2 (C), 130.6 (2xCH), 127.9 (2xCH), 127.4 (2xCH), 124.6 (2xCH), 123.2 (CH), 119.8 (CH_2), 24.9 (CH_3), 19.9 (CH_3); IR (ATR, cm^{-1}): 2990, 1728, 1649, 1572, 1379, 1253, 1195; HRESIMS calcd. for $[C_{18}H_{17}NO_4S + Na]^+$: 366.0776, found: 366.0781.

4. Conclusions

The reaction of o aryl propargyl ether **1** and p-toluenesulfonyl azide **2** in the presence of catalytic amounts of copper(I) salicylate afforded acrylimidate **3,** which was derived from a consecutive process, which involved a CuAAC reaction, a ketenimine formation and subsequent rearrangement. These elements suggest that this kind of compound will enjoy widespread application.

Supplementary Materials: The following are available online. Figure S1. FTIR spectrum for imidate **3**. Figure S2. HRESIMS spectrum for imidate **3**. Figure S3. ^{1}H NMR spectrum for imidate **3** ($CDCl_3$, 300 MHz). Figure S4. $^{13}C\{^{1}H\}$ NMR spectrum for imidate **3** ($CDCl_3$, 75 MHz).

Author Contributions: Conceptualization, E.C.-Y.; methodology, F.M.E.-M., R.E.G.-C., A.C.-C. and D.M.-O.; software, A.C.-C.; validation, F.M.E.-M. and R.E.G.-C.; formal analysis, A.C.-C. and R.E.G.-C.; investigation, R.E.G.-C.; resources, M.V.B.U. and E.C.-Y.; data curation, R.E.G.-C., A.C.-C. and D.M.-O.; writing—original draft preparation, E.C.-Y.; writing—review and editing, E.C.-Y.; visualization, M.V.B.U. and E.C.-Y.; supervision, M.V.B.U. and E.C.-Y.; project administration, M.V.B.U. and E.C.-Y.; funding acquisition, M.V.B.U. and E.C.-Y. All authors have read and agreed to the published version of the manuscript.

Funding: This research was funded by CONACYT-Mexico, project No. A1-S-18230 and project No. 319851, as well as fellowships for F.M.E.-M. (CVU: 783506) and R.E.G.-C. (CVU: 229559). This work was also supported by COMECYT (fellowship for A.C.-C.).

Institutional Review Board Statement: Not applicable.

Informed Consent Statement: Not applicable.

Data Availability Statement: Not applicable.

Acknowledgments: Financial support from CONACYT is gratefully acknowledged. The authors would like to thank N. Zavala, A. Nuñez, L. Triana and M. C. Martínez for the technical support.

Conflicts of Interest: The authors declare no conflict of interest.

References

1. Jeong Yoo, E.J.; Ahlquist, M.; Bae, I.; Sharpless, K.B.; Fokin, V.V.; Chang, S. Mechanistic Studies on the Cu-Catalyzed Three-Component Reactions of Sulfonyl Azides, 1-Alkynes and Amines, Alcohols, or Water: Dichotomy via a Common Pathway of the article. *J. Org. Chem.* **2008**, *73*, 5520–5528.
2. Kim, S.H.; Park, S.H.; Choi, J.C.; Chang, S. Sulfonyl and Phosphoryl Azides: Going Further Beyond the Click Realm of Alkyl and Aryl Azides. *Chem. Asian J.* **2011**, *6*, 2618–2634. [CrossRef] [PubMed]
3. Valencia, R.A.; Corona, D.; Cuevas-Yañez, E. Effect of the ligand in the Synthesis of 1-Sulfonyl-1,2,3-triazoles through Copper-Catalyzed Alkyne-Azide Cycloaddition. *J. Mex. Chem. Soc.* **2012**, *56*, 152–155. [CrossRef]
4. García-Vanegas, J.J.; Rodríguez-Florencio, J.; Cifuentes-Castañeda, D.D.; Mendieta-Zerón, H.; Pavón-Romero, S.; Morales-Rodríguez, M.; Corona-Becerril, D.; Cuevas-Yañez, E. Synthesis and antifungal activity evaluation of 1-sulfonyl-1,2,3-triazoles. *Pharm. Chem. J.* **2021**, *55*, 566–569. [CrossRef]
5. Cervantes-Reyes, A.; García-Vanegas, J.J.; Lopez-Téllez, G.; Hernández-Balderas, U.; García-Eleno, M.A.; Morales-Morales, D.; Cuevas-Yañez, E. Facile synthesis of copper(I) salicylate and its use in the selective synthesis of 1-acyloxy-1,2,3-triazoles and 1-sulfonyl-1,2,3-triazoles. *J. Coord. Chem.* **2022**, *75*, 729–737. [CrossRef]
6. Hisamatsu, S.; Masu, H.; Azumaya, I.; Takahashi, M.; Kishikawa, K.; Kohmoto, S. U-Shaped Aromatic Ureadicarboxylic Acids as Versatile Building Blocks: Construction of Ladder and Zigzag Networks and Channels. *Cryst. Growth Des.* **2011**, *11*, 5387–5395. [CrossRef]
7. Guo, Y.D.; Yan, X.H.; Xiao, Y.; Liu, C.S. U-shaped relationship between current and pitch in helicene molecules. *Sci. Rep.* **2015**, *5*, 16731. [CrossRef]
8. Kumar, G.R.; Kumar, Y.K.; Kant, R.; Reddy, M.S. Tandem Cu-catalyzed ketenimine formation and intramolecular nucleophile capture: Synthesis of 1,2-dihydro-2-iminoquinolines from 1-(*o*-acetamidophenyl)propargyl alcohols. *Beilstein J. Org. Chem.* **2014**, *10*, 1255–1260. [CrossRef]
9. Kumar, Y.K.; Kumar, G.R.; Reddy, M.S. Cu-Catalyzed Conversion of Propargyl Acetates to E-α,β-Unsaturated Amides via Ketenimine Formation with Sulfonyl Azides. *J. Org. Chem.* **2014**, *79*, 823–828. [CrossRef]
10. Chauhan, D.P.; Varma, S.J.; Vijeta, A.; Banerjee, P.; Talukdar, P. A 1,3-amino group migration route to form acrylamidines. *Chem. Commun.* **2014**, *50*, 323–325. [CrossRef]
11. Bruker. *APEX2, SAINT, & SADABS*; Bruker AXS Inc.: Madison, WI, USA, 2009.
12. Sheldrick, G.M. A short history of SHELX. *Acta Crystallogr. A* **2008**, *64*, 112–122. [CrossRef]
13. Sheldrick, G.M. Crystal structure refinement with SHELXL. *Acta Crystallogr. C* **2015**, *71*, 3–8. [CrossRef]
14. Hübschle, C.B.; Sheldrick, G.M.; Dittrich, B. ShelXle: A Qt graphical user interface for SHELXL. *J. Appl. Crystallogr.* **2011**, *44*, 1281–1284. [CrossRef]
15. Macrae, C.F.; Sovago, I.; Cottrell, S.J.; Galek, P.T.A.; Mccabe, P.; Pidcock, E.; Platings, M.; Shields, G.P.; Stevens, J.S.; Towler, M.; et al. Mercury 4.0: From visualization to analysis, design and prediction. *J. Appl. Crystallogr.* **2020**, *53*, 226–235. [CrossRef]
16. Cason, C.; Fröhlich, T.; Lipka, C. Persistence of Vision Raytracer. 2013. Available online: http://www.povray.org/ (accessed on 1 January 2020).

17. Frisch, M.J.; Trucks, G.W.; Schlegel, H.B.; Scuseria, G.E.; Robb, M.A.; Cheeseman, J.R.; Scalmani, G.; Barone, V.; Petersson, G.A.; Nakatsuji, H.; et al. Gaussian 16 Rev. C.01, Wallingford, CT. 2016. Available online: https://www.scirp.org/(S(lz5mqp453ed%20snp55rrgjct55))/reference/referencespapers.aspx?referenceid=2418053 (accessed on 1 January 2020).
18. Adamo, C.; Barone, V. Toward reliable density functional methods without adjustable parameters: The PBE0 model. *J. Chem. Phys.* **1999**, *110*, 6158–6170. [CrossRef]
19. Dunning, T.H. Gaussian basis sets for use in correlated molecular calculations. I. The atoms boron through neon and hydrogen. *J. Chem. Phys.* **1989**, *90*, 1007–1023. [CrossRef]
20. Woon, D.E.; Dunning, T.H. Gaussian basis sets for use in correlated molecular calculations. *III. The atoms aluminum through argon. J. Chem. Phys.* **1993**, *98*, 1358–1371.
21. Spackman, P.R.; Turner, M.J.; Mckinnon, J.J.; Wolff, S.K.; Grimwood, D.J.; Jayatilaka, D.; Spackman, M.A. CrystalExplorer: A program for Hirshfeld surface analysis, visualization and quantitative analysis of molecular crystals. *J. Appl. Crystallogr.* **2021**, *54*, 1006–1011. [CrossRef]
22. Bader, R.F.W. A Quantum Theory of Molecular Structure and Its Applications. *Chem. Rev.* **1991**, *91*, 893–928. [CrossRef]
23. Johnson, E.R.; Keinan, S.; Mori-Sánchez, P.; Contreras-García, J.; Cohen, A.J.; Yang, W. Revealing Noncovalent Interactions. *J. Am. Chem. Soc.* **2010**, *132*, 6498–6506. [CrossRef]
24. Lu, T.; Chen, F. Multiwfn: A Multifunctional Wavefunction Analyzer. *J. Comput. Chem.* **2012**, *33*, 580–592. [CrossRef] [PubMed]
25. Humphrey, W.; Dalke, A.; Schulten, K. VMD: Visual molecular dynamics. *J. Mol. Graphics* **1996**, *14*, 33–38. [CrossRef] [PubMed]
26. Williams, T.; Kelley, C.; Bersch, C.; Bröker, H.-B.; Campbell, J.; Cunningham, R.; Denholm, D.; Elber, G.; Fearick, R.; Grammes, C.; et al. gnuplot 5.2: An Interactive Plotting Program. 2019. Available online: http://www.gnuplot.info (accessed on 1 January 2020).